Reversible Clustering of Gold Nanoparticles under Confinement

Ana Sánchez-Iglesias, Nathalie Claes, Diego M. Solís, Jose M. Taboada, Sara Bals, Luis M. Liz-Marzán,* and Marek Grzelczak*

Abstract: *A limiting factor of solvent-induced nanoparticle self-assembly is the need for constant sample dilution in assembly/disassembly cycles. Changes in the nanoparticle concentration alter the kinetics of the subsequent assembly process, limiting optical signal recovery. Herein, we show that upon confining hydrophobic nanoparticles in permeable silica nanocapsules, the number of nanoparticles participating in cyclic aggregation remains constant despite bulk changes in solution, leading to highly reproducible plasmon band shifts at different solvent compositions.*

Controlling the spatial distribution of nanoparticles in the liquid phase is a convenient strategy for the bottom-up fabrication of dynamic materials.[1,2] In this context, we need stimuli that can drive the assembly/disassembly process. The list of available stimuli constantly increases, and includes electromagnetic fields (magnetic fields,[3] light),[4,5] temperature,[6,7] pH,[8,9] metal ions,[10] (bio)molecules,[11,12] and solvent composition.[13–15] The use of solvent as a stimulus has been proposed by Kumacheva and co-workers,[13] who used hydrophobic polystyrene (PS) capping agents to provide

[*] A. Sánchez-Iglesias, Prof. L. M. Liz-Marzán
CIC biomaGUNE and CIBER-BBN
Paseo de Miramón 182, 2014 Donostia-San Sebastián (Spain)
E-mail: llizmarzan@cicbiomagune.es

N. Claes, Prof. S. Bals
Electron Microscopy for Materials Science (EMAT)
Department Physics, University of Antwerp
Groenenborgerlaan 171, 2020 Antwerp (Belgium)

Dr. J. M. Taboada
Departamento de Tecnología de los Computadores y de las Comunicaciones
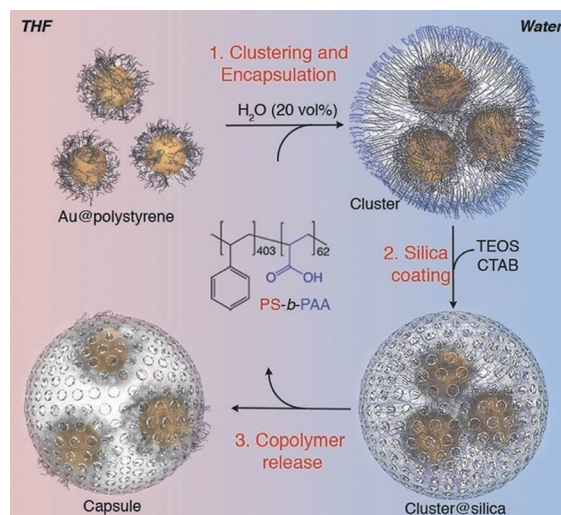University of Extremadura, 10003 Cáceres (Spain)

Dr. D. M. Solís
Departamento de Teoría de la Señal y Comunicaciones
University of Vigo, 36301 Vigo (Spain)

Dr. M. Grzelczak
Donostia International Physics Center (DIPC)
Manuel de Lardizabal 4, 20018 Donostia-San Sebastián (Spain)
E-mail: marek.grzelczak@dipc.org

Prof. L. M. Liz-Marzán, Dr. M. Grzelczak
Ikerbasque, Basque Foundation for Science
48013 Bilbao (Spain)

colloidal stability to nanoparticles in tetrahydrofuran (THF), *N*,*N*-dimethylformamide (DMF), or dioxane. Addition of water resulted in a self-assembly process driven by hydrophobic forces.[16] Despite the wide variety of experimental examples, the use of solvents to trigger assembly and disassembly hinders the switching ability, which is, however, readily achievable with other stimuli, such as light.[4] This is due to the fact that the alternate assembly/disassembly steps require increasing sample dilution. The volume changes during subsequent cycles alter the particle concentration and in turn the kinetics of the assembly process, leading to poor reproducibility. Thus, to control solvent-induced self-assembly, the number of nanoparticles involved in the cyclic aggregation needs to be kept constant, regardless of bulk changes in the solvent composition. Such a scenario cannot be realized with currently available experimental models.

The central hypothesis behind our work is based on the confinement of polystyrene-stabilized gold nanoparticles within permeable (mesoporous silica) capsules to fix the number of self-assembling nanoparticles, which results in highly reproducible shifts of the localized surface plasmon resonance (LSPR). By combining 3D characterization by electron tomography and numerical simulations, we were able to confirm that the experimentally observed plasmon shifts correlate with optical changes for individual aggregates.

Figure 1 schematically describes the fabrication of permeable capsules carrying hydrophobic gold nanoparticles: 1) PS-stabilized gold nanoparticles (in THF) form clusters

Figure 1. Fabrication of capsules containing Au NP clusters. 1) Polystyrene-capped gold nanoparticles aggregate upon addition of water and are encapsulated in polymeric micelles. 2) The polymer-encapsulated clusters are coated with mesoporous silica. 3) The block copolymer is removed by resuspension in THF.

upon water addition, and are subsequently encapsulated within a block-copolymer micelle. 2) The resulting polymeric micelles are then coated with a rigid shell of mesoporous silica. 3) The block copolymers are finally removed by resuspending the capsules in THF, which yields hollow capsules filled with hydrophobic nanoparticles.

We first synthesized gold nanoparticles (40.8 ± 1.7 nm; Figure 2, see also the Supporting Information, Figure S1) capped with benzyldimethylhexadecylammonium chloride (BDAC), which was exchanged for thiolated polystyrene
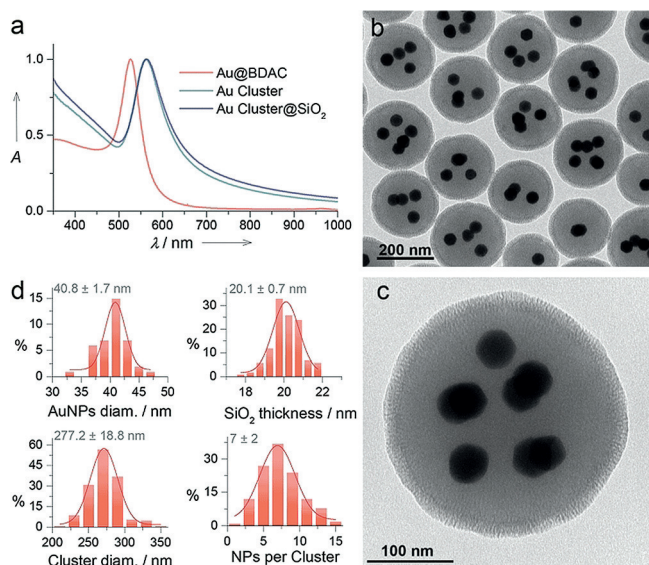

Figure 2. Nanoparticle clustering. a) Normalized UV/Vis/NIR spectra of nanoparticles before and after clustering and upon silica coating. All spectra were recorded in water to facilitate comparison. b, c) TEM images of cluster@SiO$_2$ at different magnifications. d) Histograms showing the distributions in the diameters of nanoparticles and clusters, as well as in the silica shell thickness and the number of particles per cluster.

(53 kg mol^{-1}).[14] Next, we induced nanoparticle clustering and encapsulation within polymeric micelles as described in our previous work.[17] Typically, the addition of water (20 vol%) to colloidally stable polystyrene-coated gold nanoparticles (Au@PS) in THF resulted in aggregation/clustering, which was quenched after 3 min by addition of the polymeric surfactant polystyrene-*block*-poly(acrylic acid) (PS-*b*-PAA; Figure S2). This process resulted in quasi-monodisperse plasmonic micelles (clusters, 277.2 ± 18.8 nm in diameter) containing 7 ± 2 AuNPs with long-term colloidal stability in water. The clusters were then coated with mesoporous silica (20.1 ± 0.7 nm thick), and displayed radially oriented pores (pore diameter ca. 4 nm; Figure 2b,c). The LSPR band of BDAC-stabilized Au nanoparticles was red-shifted from 527 to 564 nm upon clustering, accompanied by an increase in the extinction coefficient over the entire spectral range, which is due to significantly increased scattering. Deposition of the silica shell did not affect the position of the LSPR band but caused a small further increase in extinction (Figure 2a).

As silica is known to gradually hydrolyze and dissolve in aqueous solution,[18] we passivated cluster@SiO$_2$ particles by

silanization with a silane-terminated poly(ethylene glycol) derivative (Si-PEG, $M_n = 10\,000$ g mol^{-1}; see the Supporting Information).[19] This coating led to an increase in the hydrodynamic diameter from 322.3 ± 2.5 to 357.2 ± 2.2 nm, with no change in the zeta potential (-40 mV) and without altering the composition of the polymeric micelle (Figure S3). Evaluation of the long-term stability (1 month) of PEGylated cluster@SiO$_2$ in water confirmed the absence of structural and optical changes.

On the other hand, resuspension of cluster@SiO$_2$ in THF resulted in the diffusion of block-copolymer molecules into the bulk solution through the mesoporous silica shell. To gain insight into the kinetics of this process, we monitored the copolymer release by UV/Vis/NIR spectroscopy (Figure 3a).
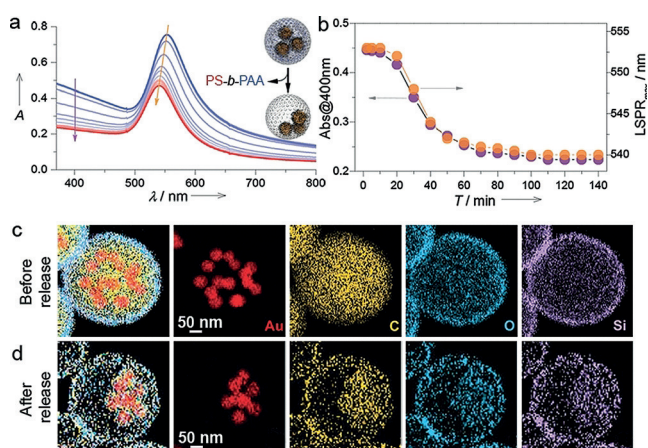
Figure 3. Formation of capsules through block-copolymer extraction. a) Time-dependent UV/Vis/NIR spectra of encapsulated clusters in THF. b) Changes in the absorbance at 400 nm and the LSPR maximum during incubation in THF. c) STEM-EDX elemental analysis of encapsulated clusters (before and after block-copolymer extraction), showing a decrease in the carbon signal.

The extinction was observed to gradually decrease, accounting for decreased scattering, but reached a plateau after 2 h. By plotting the absorbance at 400 nm (Abs@400) versus incubation time, we observed an induction time of 10 min and a subsequent drop in absorbance corresponding to copolymer extraction, which is completed after 2 h (Figure 3b). We also observed an LSPR blue-shift from 553 to 539 nm (Figure 3b), which is due to a decrease in the local refractive index (from 1.59 for polystyrene to 1.40 for THF) and to increased interparticle distances. The LSPR maximum of empty capsules in THF had a similar value to that of free Au@PS in the same solvent (Figure S4), suggesting that the particles are not aggregated inside the capsule. Time-dependent TEM characterization confirmed gradual block-copolymer extraction through an increase in the contrast inside the capsules (Figure S5). We also implemented STEM-EDX elemental analysis to visualize the changes in carbon intensity before and after copolymer release, while the distributions of other elements (Si, O, Au) remained unchanged (Figure 3c,d).

Reversible aggregation of Au@PS within the capsules was tested by repeatedly varying the water content. Because of

the sample dilution in each aggregation step (H$_2$O addition), the initial solvent composition (pure THF) cannot be recovered during disassembly (THF addition). Therefore, we defined lower (5 vol%) and upper (40 vol%) limits of water concentration, at which the LSPR band would be fully blue-shifted (dispersed) and fully red-shifted (aggregated), respectively (Figure S6). We performed 15 aggregation cycles by alternating the amount of water between 5 and 50 vol% (water excess to ensure the full red-shift), obtaining highly reproducible spectral features. Not only did the LSPR maximum oscillate between 542 and 572 nm with high precision, but the full width at half maximum (FWMH) also oscillated between 88 and 155 nm (Figure 4d,e). TEM analysis at the limiting water contents confirmed the structures expected from the measured optical spectra; Au@PS remained dispersed in the capsules at 5 vol% water, but aggregated at 50 vol% (Figure 4a,b). The exceptional LSPR switching ability arises from the constant number of particles participating in the aggregation process (ca. 7 for each cluster).

We additionally observed that nanoparticle confinement in the capsules resulted in an increased aggregation rate, as compared to free nanoparticles in solution. Whereas it took less than 3 min for the LSPR band to be fully red-shifted in

the confined nanoparticles, the aggregation of free Au@PS at the same water content (20 vol%) took nearly 20 min (Figure 4f). This is likely due to the decreased initial interparticle distances under confinement, which allows for faster aggregation.

To further demonstrate the ability of this system to switch its optical response, we immobilized the loaded capsules on a solid (glass) substrate for fast handling in and out of different solvents. By using a conventional layer-by-layer method,[20] we functionalized a glass slide with a cationic polyelectrolyte, and immobilized the capsules on this slide through electrostatic interactions. A single layer of capsules was enough to impose a visible coloration to the glass. Cyclic immersion of the substrate in THF and water produced optical changes that were readily detected by the naked eye and confirmed by measuring the spectral shifts (Figures 4g and S7). It should be noted that during these experiments, the humidity in our laboratory was 80% (conditioned by the weather in Donostia-San Sebastian in mid-August), so that the particles remained aggregated when stored in solution-free conditions. Exposure of the supported capsules to THF vapor led to an immediate color change from blue to red, as a result of the THF-rich atmosphere (Figure 4h; for videos showing the color switching of a glass slide, see Movies S1 and S2). Facile substrate handling and reproducible optical responses pave the way towards the design of colorimetric sensors for humidity, volatile solvents, or small hydrophobic molecules.

In this case, reversible assembly involves seven nanoparticles on average, thereby resulting in highly reproducible plasmon shifts. As a consequence, the LSPR shifts of individual capsules are expected to reflect the LSPR shift of the bulk sample. Therefore, numerical simulations of the spectral changes for dispersed and aggregated particles inside a capsule should faithfully reproduce the experimental optical changes. We employed 3D electron tomography to acquire an accurate representation of the spatial distribution of Au@PS in randomly selected capsules containing both aggregated and dispersed nanoparticles at specific solvent compositions (Figure 5a and Movies S3 and S4). Accurate 3D coordinates obtained from 3D electron tomography (3D models in Figure 5b) were directly used as the input for simulations of the extinction spectra by a reported method based on surface integral equations with the method-of-moments formulation.[21] This process enables time-effective simulations of arbitrary complex nanostructures (in this case including the nanoparticles at specific positions, the silica shell, and the solvent; see the Supporting Information for details). Even though the selected capsules differed in the overall diameter and the number of Au@PS particles, the obtained numerical extinction spectra accurately resemble the experimental absorbance spectra of the solution in the same solvents. For the simulated spectra in THF, the LSPR maximum was located at 538 nm while in water it was found at 572 nm (Figure 5e,f); these values are in good agreement with the experimental data (540 nm for THF and 572 nm for water). Again, the good correlation between simulated and experimental data is due to the invariant number of particles involved in the aggregation process. It should be noted that
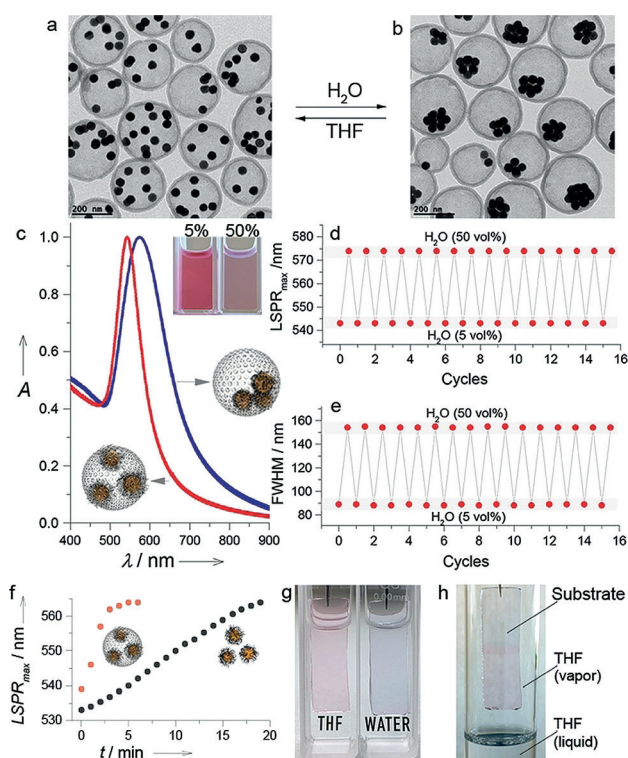
Figure 4. Reversible optical switching. a,b) TEM images of capsules with low and high water content (5 vol% (a); 50 vol% (b)). c) UV/Vis/NIR spectra of the capsules during cyclic addition of water and THF. d,e) Evolution of the LSPR maximum (d) and the FWHM (e) over 15 cycles. f) Aggregation kinetics of confined and free Au@PS, at the same nanoparticle concentration and water content (20 vol%). g) Photographs showing a capsule-functionalized glass substrate in THF (red) and in water (blue). h) Photograph of a capsule-functionalized glass slide exposed to vapor from warm THF, leading to a fast color change.
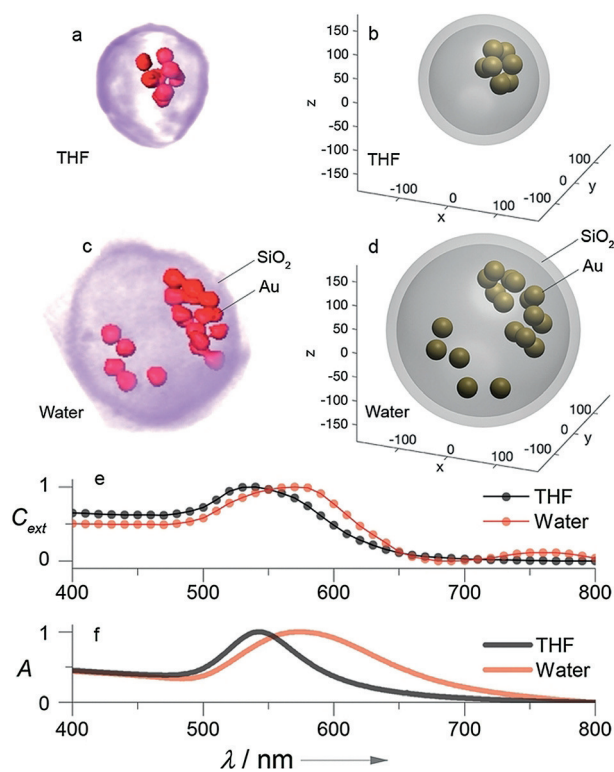
Figure 5. Numerical simulation of the LSPR shift. a,c) 3D electron tomography rendering of randomly selected capsules in water (a) and in THF (c). b,d) 3D models constructed from the coordinates obtained by 3D electron tomography. The models served as an input for numerical calculations of spectra. e) Calculated extinction spectra of clusters in THF and in water. f) Experimental spectra, showing good correlation of the LSPR positions.

the numerical spectra confirmed that the presence of the silica shell does not affect the optical response in THF because of the similar refractive indices of SiO_2 (1.47) and THF (1.40).

In conclusion, we have demonstrated that the confinement of gold nanoparticles in permeable silica shells allows for highly reproducible clustering at different solvent compositions as the number of particles participating in the aggregation process remains constant. Our method shows unprecedented optical signal switching during the solvent-induced reversible clustering of nanoparticles. The structural advantage of our method is based on the fact that the nanoparticles are not loaded into a predefined container; instead, the container is built around as-prepared clusters, avoiding issues related to cargo leakage. Incidentally, our method is also cost-efficient as the copolymer can be recovered for subsequent encapsulation processes.

Conflict of interest

The authors declare no conflict of interest.

[1] B. A. Grzybowski, K. Fitzner, J. Paczesny, S. Granick, *Chem. Soc. Rev.* **2017**, *46*, 5647–5678.
[2] Z. Nie, A. Petukhova, E. Kumacheva, *Nat. Nanotechnol.* **2010**, *5*, 15–25.
[3] K. Butter, P. H. H. Bomans, P. M. Frederik, G. J. Vroege, A. P. Philipse, *Nat. Mater.* **2003**, *2*, 88–91.
[4] R. Klajn, K. J. M. Bishop, B. A. Grzybowski, *Proc. Natl. Acad. Sci. USA* **2007**, *104*, 10305–10309.
[5] P. K. Kundu, D. Samanta, R. Leizrowice, B. Margulis, H. Zhao, M. Börner, T. Udayabhaskararao, D. Manna, R. Klajn, *Nat. Chem.* **2015**, *7*, 646–652.
[6] Y. Liu, X. Han, L. He, Y. Yin, *Angew. Chem. Int. Ed.* **2012**, *51*, 6373–6377; *Angew. Chem.* **2012**, *124*, 6479–6483.
[7] S. Balasubramaniam, N. Pothayee, Y. Lin, M. House, R. C. Woodward, T. G. St. Pierre, R. M. Davis, J. S. Riffle, *Chem. Mater.* **2011**, *23*, 3348–3356.
[8] D. Wang, B. Kowalczyk, I. Lagzi, B. A. Grzybowski, *J. Phys. Chem. Lett.* **2010**, *1*, 1459–1462.
[9] L. Heinen, T. Heuser, A. Steinschulte, A. Walther, *Nano Lett.* **2017**, *17*, 4989–4995.
[10] S. Si, M. Raula, T. K. Paira, T. K. Mandal, *ChemPhysChem* **2008**, *9*, 1578–1584.
[11] K. L. Gurunatha, A. C. Fournier, A. Urvoas, M. Valerio-Lepiniec, V. Marchi, P. Minard, E. Dujardin, *ACS Nano* **2016**, *10*, 3176–3185.
[12] G. von Maltzahn, D.-H. Min, Y. Zhang, J.-H. Park, T. J. Harris, M. Sailor, S. N. Bhatia, *Adv. Mater.* **2007**, *19*, 3579–3583.
[13] Z. Nie, D. Fava, E. Kumacheva, S. Zou, G. C. Walker, M. Rubinstein, *Nat. Mater.* **2007**, *6*, 609–614.
[14] A. Sánchez-Iglesias et al., *ACS Nano* **2012**, *6*, 11059–11065.
[15] H. Hu et al., *ACS Nano* **2016**, *10*, 7323–7330.
[16] R. M. Choueiri, A. Klinkova, H. Thérien-Aubin, M. Rubinstein, E. Kumacheva, *J. Am. Chem. Soc.* **2013**, *135*, 10262–10265.
[17] M. Grzelczak, A. Sánchez-Iglesias, L. M. Liz-Marzán, *CrystEngComm* **2014**, *16*, 9425–9429.
[18] H. Yamada, C. Urata, Y. Aoyama, S. Osada, Y. Yamauchi, K. Kuroda, *Chem. Mater.* **2012**, *24*, 1462–1471.
[19] V. Cauda, C. Argyo, T. Bein, *J. Mater. Chem.* **2010**, *20*, 8693–8699.
[20] I. Pastoriza-Santos, A. Sánchez-Iglesias, F. J. García de Abajo, L. M. Liz-Marzán, *Adv. Funct. Mater.* **2007**, *17*, 1443–1450.
[21] D. M. Solís, J. M. Taboada, F. Obelleiro, L. M. Liz-Marzán, F. J. García de Abajo, *ACS Nano* **2014**, *8*, 7559–7570.